university of groningen

University Medical Center Groningen

University of Groningen

Cluster evolution and critical cluster sizes for the square and triangular lattice Ising models using lattice animals and Monte Carlo simulations

Eising, G.; Kooi, B. J.

Published in:
Physical Review. B: Condensed Matter and Materials Physics

DOI:
10.1103/PhysRevB.85.214108

IMPORTANT NOTE: You are advised to consult the publisher's version (publisher's PDF) if you wish to cite from it. Please check the document version below.

Document Version
Publisher's PDF, also known as Version of record

Publication date:
2012

Link to publication in University of Groningen/UMCG research database

Citation for published version (APA):
Eising, G., & Kooi, B. J. (2012). Cluster evolution and critical cluster sizes for the square and triangular lattice Ising models using lattice animals and Monte Carlo simulations. *Physical Review. B: Condensed Matter and Materials Physics*, *85*(21), 214108-1-214108-12. [214108].
https://doi.org/10.1103/PhysRevB.85.214108

Copyright
Other than for strictly personal use, it is not permitted to download or to forward/distribute the text or part of it without the consent of the author(s) and/or copyright holder(s), unless the work is under an open content license (like Creative Commons).

The publication may also be distributed here under the terms of Article 25fa of the Dutch Copyright Act, indicated by the “Taverne” license. More information can be found on the University of Groningen website: https://www.rug.nl/library/open-access/self-archiving-pure/taverne-amendment.

Take-down policy
If you believe that this document breaches copyright please contact us providing details, and we will remove access to the work immediately and investigate your claim.

Downloaded from the University of Groningen/UMCG research database (Pure): http://www.rug.nl/research/portal. For technical reasons the number of authors shown on this cover page is limited to 10 maximum.

Cluster evolution and critical cluster sizes for the square and triangular lattice Ising models using lattice animals and Monte Carlo simulations

G. Eising* and B. J. Kooi†

Zernike Institute for Advanced Materials and the Materials innovation institute M2i, University of Groningen, 9747 AG Groningen, The Netherlands

(Received 7 December 2011; revised manuscript received 29 March 2012; published 8 June 2012)

Growth and decay of clusters at temperatures below T_c have been studied for a two-dimensional Ising model for both square and triangular lattices using Monte Carlo (MC) simulations and the enumeration of lattice animals. For the lattice animals, all unique cluster configurations with their internal bonds were identified up to 25 spins for the triangular lattice and up to 29 spins for the square lattice. From these configurations, the critical cluster sizes for nucleation have been determined based on two (thermodynamic) definitions. From the Monte Carlo simulations, the critical cluster size is also obtained by studying the decay and growth of inserted, most compact clusters of different sizes. A good agreement is found between the results from the MC simulations and one of the definitions of critical size used for the lattice animals at temperatures $T > \sim 0.4\ T_c$ for the square lattice and $T > \sim 0.2\ T_c$ for the triangular lattice (for the range of external fields H considered). At low temperatures ($T \approx 0.2\ T_c$ for the square lattice and $T \approx 0.1\ T_c$ for the triangular lattice), magic numbers are found in the size distributions during the MC simulations. However, these numbers are not present in the critical cluster sizes based on the MC simulations, as they are present for the lattice animal data. In order to achieve these magic numbers in the critical cluster sizes based on the MC simulation, the temperature has to be reduced further to $T \approx 0.15\ T_c$ for the square lattice. The observed evolution of magic numbers as a function of temperature is rationalized in the present work.

DOI: 10.1103/PhysRevB.85.214108 PACS number(s): 64.60.qe, 64.60.De, 02.70.Uu, 64.60.My

I. INTRODUCTION

Understanding nucleation processes is of great importance, because many natural and technological processes critically depend on nucleation. Most phase transformations proceed via nucleation and growth, and such transitions occur in a wide variety of systems from atomic to astronomic length scales. For instance, stars and solar systems have been developed in the (early) universe by nucleation and growth.[1] Clouds and rain drops can be associated with nucleation and growth.[2] Nucleation plays also a key role in most materials production, having in general a crucial influence on the final product performance, for instance, determining crystal grain sizes and morphologies, second-phase precipitation, recrystallization, etc.[3–5]

A crucial ingredient of nucleation is the presence of an energy barrier that has to be overcome by multiple crossing attempts by certain jump frequencies with certain energies (which often is the thermal energy). The energy barrier is directly associated with (the minimal work required to form) a critical nucleus. For sizes smaller than this critical one, the nucleus has a larger probability to decay than grow, and this is only reversed when a nucleus size becomes larger than the critical one. The attempts to cross the energy barrier can in many systems be described as a stepwise release or attachment of monomers to clusters ranging in size from a single monomer to a size that exceeds the critical cluster size having a number of monomers n^*. In the isotropic case, cluster properties are only a function of the number of monomers (spins, atoms, etc.) n they contain. Clusters decay or grow by stepwise release or attachment of a monomer ($n-1$ and $n+1$), i.e., the process is a one-dimensional Markov chain. Although a complete picture of (both steady state and transient) nucleation is far from trivial in this one-dimensional case,[6] the complexity strongly increases when clusters with the same n can have a large variety in shapes and energies, as is already the case within the relatively simple 2D square lattice Ising model for $n \geqslant 6$.[7–9] For example, for $n = 19$, 20, and 21, the total number of distinct cluster configurations on the 2D square lattice is over 5.9×10^9, 22×10^9, and 88×10^9, respectively.[9] In principle, all possible transitions with their energies and probabilities between all configurations for such $n-1 \leftrightarrow n \leftrightarrow n+1$ have to be considered from $n = 0$ to n clearly larger than the critical nucleus size n^* in order to arrive at a complete picture of nucleation. Fortunately, the situation simplifies at low temperatures, because cluster energy will prevail over entropy, and thus, for each n, only clusters with the lowest possible energies have to be considered. Then, most configurations can be discarded and the one-dimensional case is again approached. For instance, for $n =$ 19, 20, and 21, the number of clusters with the lowest energy (two lowest energies) is 8 (922), 2 (428), and 187 (7835), respectively.[9]

Interesting work has been published recently on the validity of the classical nucleation theory for Ising models.[10] However, still the nucleation process is considered a 1D Markov. The present work shows that in principle this one-dimensionality is valid when (i) growth proceeds only along the lowest possible energy path at very low temperatures and (ii) at sufficiently high temperatures, the anisotropy in surface energy vanishes.

These examples shows that dynamic Ising models can be relevant and have been popular systems for studying and understanding nucleation (see a nonexhaustive list in Refs. 8–14). Also, the present work is dedicated to this field of research by

 ©2012 American Physical Society

studying for the 2D square and triangular lattice Ising models the critical cluster for nucleation. Two thermodynamic and one kinetic definition have been used to determine the critical cluster size as a function of the external magnetic field H and temperature T below T_c. The thermodynamic definitions are based on lattice animal enumeration up to $n = 29$ for the square lattice and up to $n = 25$ for the triangular lattice. Critical cluster sizes obtained in this way are compared with the ones obtained by the MC simulations based on a technique that we recently developed.[14] Since the MC simulations and the critical cluster size determination (based on the kinetic definition) are computer resource intensive, they were limited to $0.23\ T_c \leqslant T \leqslant 0.5\ T_c$ and a certain interval of H values. A striking result of the comparison is that critical cluster sizes with magic numbers are present at low temperatures ($T \approx 0.2\ T_c$ for the square lattice and $T \approx 0.1\ T_c$ for the triangular lattice) according to both thermodynamic definitions, whereas they are still absent according to the kinetic definition. Yet, the same type of magic numbers are present in the actual size distributions as obtained using the MC simulations at these low temperatures, but they do not show up in the critical cluster size according to the kinetic definition. In order to observe these magic numbers also in the critical nucleus sizes based on the kinetic definition, the temperature has to be reduced further ($T \approx 0.15\ T_c$ for the square lattice). This work shows that the actual critical nucleus involves averaging over neighboring cluster sizes and therefore can be also rationalized in the light of the so-called transition path theory.[15]

The paper is organized as follows. In Sec. II, the model and numerical methods are explained in detail. Then the results are presented in Sec. III based on the lattice animal enumerations (A), based on the Monte Carlo (MC) simulations (B). The results of Secs. III A and III B are compared in Sec. III C. Subsequently, the temperature evolutions of magic numbers according to the Monte Carlo simulations are compared for the square and triangular lattice, and finally, the correlation of these evolutions with the temperature evolution of the interface tensions for the respective Ising models is shown.

II. MODEL AND NUMERICAL METHODS

A. Ising model

We consider the standard 2D Ising model with the Hamiltonian given by

$$\mathcal{H} = -J \sum_{nn} \sigma_i \sigma_j - H \sum_i \sigma_i \tag{1}$$

with a ferromagnetic coupling constant $J > 0$ between the spins σ having ± 1 value and with an external magnetic field H; nn indicates the summation over all nearest-neighbor pairs.

The energy of a cluster with spins up on a 2D lattice with surrounding spins down in a field H pointing up is defined by the cluster size n and the number of internal nearest-neighbor bonds b:

$$E_n^b = 2J\,P_n^b - 2nH \tag{2}$$

with P_n^b the perimeter of the cluster given by

$$P_n^b = 4n - 2b \text{ for a square lattice and} \tag{3a}$$

$$P_n^b = 6n - 2b \text{ for a triangular lattice.} \tag{3b}$$

At low temperatures, growth of clusters is completely dominated by the path along minimum cluster energies and thus occurs via the most compact shapes. This means a minimum in E_n^b for each n, corresponding to a maximum in the number of bonds b for each n (being the minimal perimeter). The curve of E_n^b versus n in this case is not smooth, because it has an overall classical (Gibbs) outlook plus sharp saw-tooth modulation, see for example Fig. 6(a).

On the square lattice the square mxm and rectangular $mx(m+1)$ shapes, i.e., with $\{10\}$ facets are the most compact shapes. For a given external magnetic field H, the critical length m* is defined by $m^* =$ "floor"$(2J/H)$ with $J(>0)$ the ferromagnetic coupling constant in the standard Ising Hamiltonian [cf. Eq. (1)], where the operation "floor" means rounding to the lower nearest-integer number. The critical nucleus, as derived by Neves and Schonmann for $T \to 0$,[16] is then the $n^* = m^* x (m^* + 1)$ rectangle with an extra spin on the longer side. Directly above $T = 0$, also the intermediate $n = m^2 + 1$ clusters can become critical nuclei.[8] The higher the temperature, the more these discrete magic values of n due to the specific low-energy configurations become replaced by the continuous spectrum of all integer n values due to configurational entropy.

For the triangular lattice, this analysis of most compact shapes and the magic critical cluster sizes has not been presented before and is somewhat more complicated (than for the square lattice), but still can be derived readily based on Eqs. (2) and (3b). The curve of E_n^b versus n along the lowest-energy path shows primary minima in energy for the most compact hexagonal shapes [m(integer) $\geqslant 1$]:

$$n_p^- = 3m^2 - 3m + 1, \tag{4a}$$

$$b_p^- = 9m^2 - 15m + 6, \tag{4b}$$

$$E_n^b = 4J\left[-\frac{9H}{6J}m^2 + \left(6 + \frac{9H}{6J}\right)m - \left(6 + \frac{3H}{6J}\right)\right]. \tag{4c}$$

Similar to the square lattice, m can be interpreted physically as the facet length in this case of the hexagon. "Primary" critical fields H_p^* occur at the maximum in the primary energy minimum:

$$H_p^* = \frac{4J}{2m-1}. \tag{5}$$

In between two sequential primary critical fields, starting from $H_p^* = \frac{4J}{2m-1}$ in the direction of decreasing H values (i.e., going from m to $m+1$), first, a primary maximum occurs for

$$n_p^{+1} = 3m^2 - 2m + 1, \tag{6a}$$

$$b_p^{+1} = 9m^2 - 12m + 4. \tag{6b}$$

Secondary maxima are absent at zero Kelvin, but three secondary maxima do arise for $T > 0$, originating from the secondary critical field at $T = 0$:

$$H_s^* = \frac{6J}{3m}. \tag{7}$$

These three secondary maxima in order of decreasing H values are

$$n_s^{+2} = 3m^2 - m + 1, \tag{8a}$$
$$b_s^{+2} = 9m^2 - 9m + 3, \tag{8b}$$
$$n_s^{+3} = 3m^2 + 1, \tag{8c}$$
$$b_s^{+3} = 9m^2 - 6m + 2, \tag{8d}$$
$$n_s^{+4} = 3m^2 + m + 1, \tag{8e}$$
$$b_s^{+4} = 9m^2 - 3m + 1. \tag{8f}$$

Then the second primary maximum with

$$n_p^{+5} = 3m^2 + 2m + 1, \tag{9a}$$
$$b_p^{+5} = 9m^2 \tag{9b}$$

occurs down to the next $H_p^* = \frac{4J}{2(m+1)-1}$.

Summarizing, in between two sequential H_p^*, in the direction of decreasing H values, there are, at low temperatures, always five domains of constant critical nucleus sizes, where the first $n_p^{+1} = 3m^2 - 2m + 1$ and fifth $n_p^{+5} = 3m^2 + 2m + 1$ correspond to primary domains that at $T = 0$ span the regions defined by $\frac{4J}{2m-1} < H < \frac{6J}{3m}$ and $\frac{6J}{3m} < H < \frac{4J}{2(m+1)-1}$, respectively. The three secondary domains only emerge for $T > 0$ and they originate from $H = \frac{6J}{3m}$ at $T = 0$. One can wonder why there are only five domains and not six, because that would correspond to adding one extra spin to each of the six facets of a perfect hexagon. The reason is that the perfect hexagon has that low (cusp in) energy that adding the first extra spin to one of the six facets of the hexagon will not provide a maximum in energy and will thus not be a critical cluster size at low temperatures.

Based on the energies E_n^b, the semiequilibrium distribution (number density) D_n^b of noninteracting clusters can be derived:[8]

$$D_n^b = w_n^b \exp\left(-\frac{E_n^b}{k_B T}\right), \tag{10}$$

where k_B is the Boltzmann constant and w_n^b is the distinct number of configurations possible for given cluster size n and internal bond count b. For the square lattice, the values w_n^b can be found in literature up to $n = 21$,[9] for the triangular lattice, no relevant literature providing w_n^b values exists. Note that existing literature only provides data on the total number of configurations, polyominoes (polyiamonds, polyhexes), or lattice animals for a given n or provides data on the so-called perimeter polynomials. In the latter case, not only the total number of clusters with a certain size n is given, but also how this total number is subdivided over the various possible perimeters. The perimeter is defined as the number of adjacent unoccupied lattice sites that is not equal to the number of bonds to unoccupied nearest-neighbor sites needed to calculate the number of internal bonds. Therefore these known values cannot be used to specify w_n^b and to calculate the number distribution D_n^b, which is essential for the study of nucleation (see, e.g., Refs. 7 and 8.).

B. Lattice animal enumeration

The semiequilibrium distribution of noninteracting clusters as described by Eq. (10) is central to the present work and also can be considered fundamental for understanding the nucleation problem of clusters on a lattice (see, e.g., Refs. 7 and 8.). The energies E_n^b in Eq. (10) can be determined readily, but calculation of the w_n^b values, apart from small cluster sizes n, is very demanding. Based on algorithms by Redner[17] and Mertens,[18] a parallel algorithm was developed to enumerate all these fixed w_n^b configurations or lattice animals up to a given size $n_{\max}$ including the internal bond counts for each configuration. The enumeration was done recursively, i.e., using a cluster of size n all possible clusters of size $n + 1$ are generated using the cluster of size n as base. The $(n + 1)$ clusters are then used to generate the $(n + 2)$ clusters in a similar way. To prevent generating the same cluster multiple times, information is passed on to the $(n + 1)$ clusters on which lattice sites already have been used by previous n clusters and are thus forbidden. This is explained in more detail in Ref. 18.

As information on which lattice sites are available for $n + 1$ clusters is only provided by clusters smaller than size $n + 1$, it is possible to split the calculations into multiple branches at size n allowing for perfect paralellization.[18] First, all unique configurations up to size n are generated and stored, together with the information on available and forbidden lattice sites. Then a number of calculations is started, equal to the number of unique configurations at size n, generating all configurations of size $n + 1$ up to $n_{\max}$ with the clusters of size n as starting points.

Using this algorithm, the number of configurations w_n^b for the square lattice was calculated up to $n_{\max} = 29$ and for the triangular lattice, up to $n_{\max} = 25$. It is noted that the limit $n_{\max}$ is imposed by the available computing power, because increasing $n_{\max}$ with one would require four to five times more computing power or time as the total amount of lattice animals increases four to five times. The current enumerations used 40000 hours of CPU time on the Millipede computing cluster at the University of Groningen, which consists of 2832 Opteron 2.6 GHz cores.

C. Critical cluster sizes

Based on the semiequilibrium distribution of noninteracting clusters [see Eq. (10)], two definitions are possible for the determination of the critical cluster size for nucleation at a given temperature and external field.[8] The "microscopic" saddle-point definition identifies a maximum D_n^b among all possible b for a given n. Then a minimum among all n is selected. The second definition is a thermodynamically averaged distribution, i.e., for each n, first, averaging over all b takes place and then the optimum is selected.

Using the microscopic saddle point,[8] the critical cluster size n^* for nucleation is identified. $D_n(H,T)$ is defined as the maximum of $D_n^b(H,T)$ for a given n for all possible b:

$$D_n(H,T) = \max\left[D_n^b(H,T); b_{\min} \leqslant b \leqslant b_{\max}\right]. \tag{11a}$$

From this definition, we find the most favorable amount of bonds for a given n at a certain temperature and field. The critical cluster size $n^*(H,T)$ is then given by n for which

$D_n(H,T)$ is minimal:

$$D_{n^*}(H,T) = \min[D_n(H,T); 1 \leqslant n \leqslant n_{\max}]. \quad (11b)$$

The critical cluster size according to the thermodynamically averaged definition is derived by summing the contributions of all possible internal bond counts such that an averaged $\langle W\rangle_n(H,T)$ is obtained,

$$\langle W\rangle_n(H,T) = 12nJ(1-H/6) - k_BT\ln \times \sum_{b=b_{\min}(n)}^{b=b_{\max}(n)} w_n^b e^{4Jb/k_bT} \text{ for a triangular lattice and} \quad (12a)$$

$$\langle W\rangle_n(H,T) = 8nJ(1-H/4) - k_BT\ln \times \sum_{b=b_{\min}(n)}^{b=b_{\max}(n)} w_n^b e^{4Jb/k_bT} \text{ for a square lattice,} \quad (12b)$$

and then determining the critical size by selecting the maximum:

$$\langle W\rangle_{n^*}(H,T) = \max[\langle W\rangle_n(H,T); 1 \leqslant n \leqslant n_{\max}]. \quad (12c)$$

It is convenient to scale J and the Boltzmann constant k_B to unity and define the temperature with respect to the critical temperature T_c. Calculations were done up to 1.3 T_c, where $T_c = 2/\ln(\sqrt{2}+1)$ for the square lattice given by Onsager's exact solution[19] and $T_c = 4/\ln(3)$ for the triangular lattice.[20] Note that beyond T_c results can be readily calculated, but they do not have physical meaning and should be treated as formal.

Both definitions for the critical cluster size result in figures with domains of constant critical number n^* (with associated b^*) as function of temperature and external field. For the square lattice, this analysis and the construction of figures was already done by Ref. 8 up to $n_{\max} = 17$. For the triangular lattice, no domain map has been published before as existing literature only provides data on the total number of configurations, polyominoes (polyiamonds, polyhexes), or lattice animals for a given n or provides data on the so-called perimeter polynomials, which are not the same as our w_n^b as already explained above.

Note that both definitions of the critical cluster size can never fully agree with the exact results derived for the square lattice by Neves and Schonmann for the critical nuclei when (for fixed H) $T\to 0$. The reason is that in the lattice animal enumeration there is no distinction between the true Neves-Schonmann critical nucleus configurations and configurations that have the same size and energy. To give the most simple example, the $n = 3$ straight cluster and the $n = 3$ L-shaped cluster have the same size and energy in the lattice animal enumeration and are not distinguished, whereas only the latter is a true critical nucleus according to the exact results for $1J < H < 2J$ when $T\to 0$. Nevertheless, as will be demonstrated below, the critical nucleus sizes as a function of H for $T\to 0$ based on the two definitions given above still completely agree with the *sizes* predicted by the exact results of Neves and Schonmann.

D. Monte Carlo simulations

In order to compare critical cluster sizes derived on the basis of the definitions presented in the previous section, which employ lattice animal enumeration and have in fact a thermodynamic basis, an alternative method employing Monte Carlo simulations is introduced here, which has a kinetic basis. Cluster growth on triangular and square lattices was studied using Monte Carlo simulations using the method outlined in Ref. 14. To study the dynamic cluster evolution processes, the stochastic Glauber dynamics was used, where the spin-flip probabilities are defined by[21]

$$P[s_i \to -s_i] = \frac{\exp(-\beta\Delta E)}{1+\exp(-\beta\Delta E)} \quad (13)$$

with $\beta = 1/k_BT$, with k_B the Boltzmann constant, T the temperature, and ΔE the energy change due to the spin flip defined according to the Ising model of Eq. (1) by

$$\Delta E = 2s_i\left(J\sum_{nn} s_j + H\right) \quad (14)$$

with nn the nearest-neighbor sites of site i.

Simulations were performed on small square or triangular lattices with appropriate boundary conditions. Initially, all spins are pointing downward. For each Monte Carlo step, a site is chosen at random and flipped with the probability given in Eq. (13). Time is given in units of Monte Carlo steps per site (MCSS), i.e., in one unit, a number of Monte Carlo steps are performed that is equal to the total amount of lattice sites.

To be able to perform relevant MC simulations at low temperatures ($T < 0.5\ T_c$) and low fields ($H < 0.5$), a cluster with n spins pointing upward is inserted near the center of a relatively small lattice at $t = 0$ in order to speed up the simulation process. It was shown that inserted clusters of course show stochastic behavior.[14] However, deterministic overall behavior (e.g., the overall fractions of growing and decaying clusters and the whole size distribution after a certain number of MCSS as will be shown below) can be obtained approximately by repeating the simulations several thousand times.[14,22] The inserted clusters correspond to the most compact shapes, i.e., with the highest number of internal bonds. All the clusters of various size n considered are on the growth path associated with the most compact shapes and thus remain closest to a perfect square shape on the square lattice and a perfect hexagonal shape on the triangular lattice. However, our experiments also show that the results on the critical nuclei are not sensitive to the type of inserted cluster, because results for inserted clusters with two internal bonds less, i.e., two corner sides of the most compact clusters were removed and added to the longer sides of the remaining cluster, showed very similar results.

During the simulation, the evolution of the size of the single cluster and its number of internal bonds as a function of time is followed. After a certain number of MCSS, the amount of clusters and the cluster sizes are determined using the efficient Hoshen-Kopelman algorithm.[23] The cluster size n is defined as the total number of connected spins with a positive orientation. If multiple clusters are present, the size of the largest cluster is taken.

It was shown in Ref. 14 that early on in the simulation the distribution curves after various MCSS are pivoting around a central point that coincides with the final fraction of clusters that will decay and grow. With distribution curve we mean here

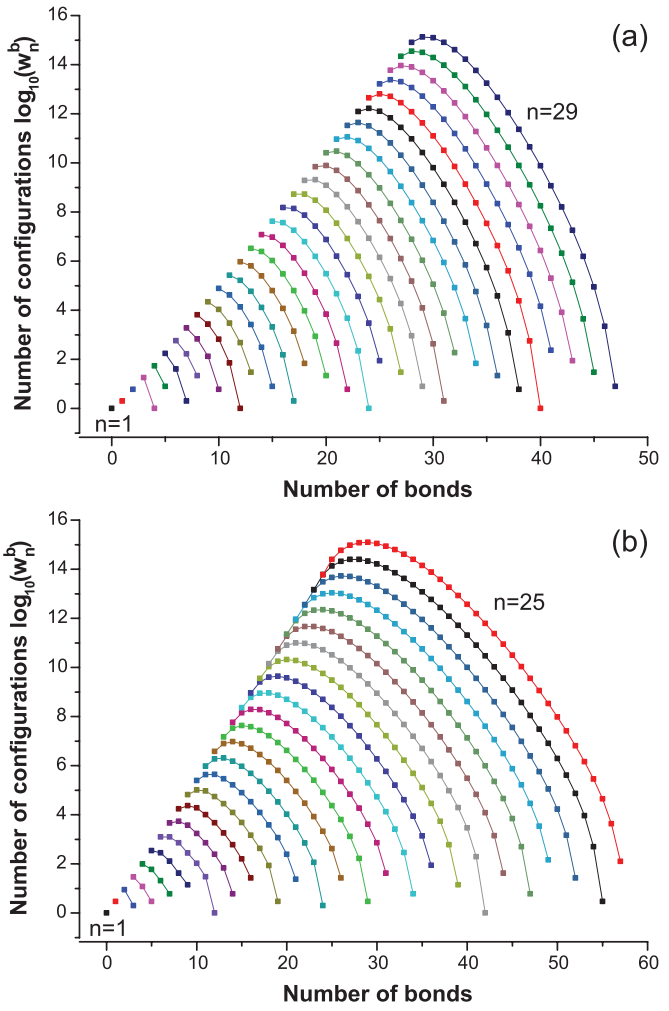

FIG. 1. (Color online) Number of configurations w_n^b as a function of the amount of bonds for clusters of given size n for the square lattice (a) and the triangular lattice (b). Solid lines connect points belonging to the same size n but having a different number of bonds b.

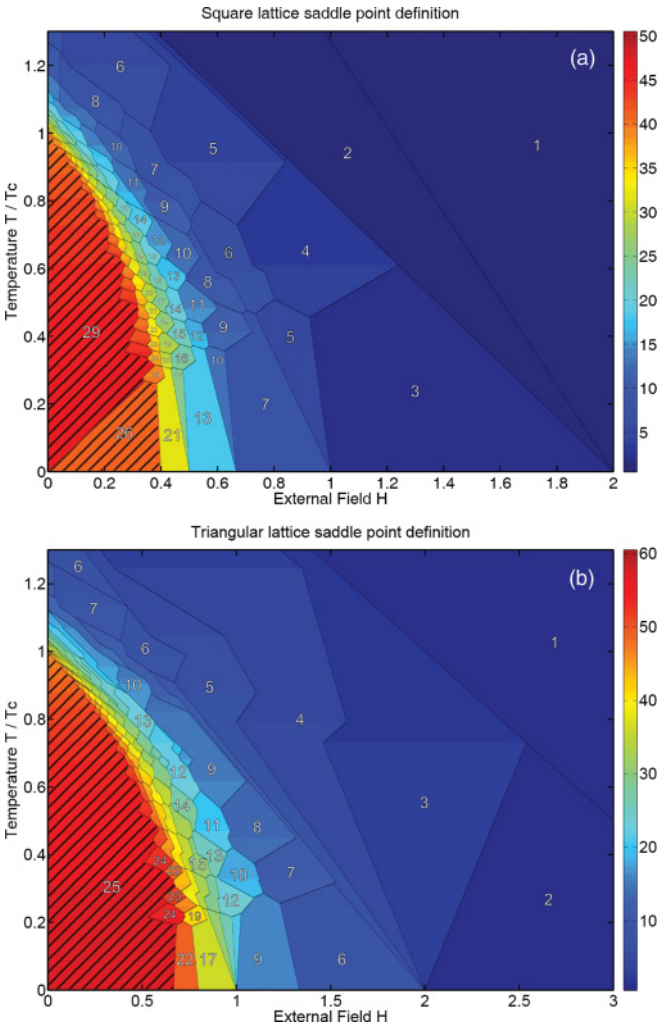

FIG. 2. (Color online) Plot of normalized temperature vs external field H showing domains with constant critical bond count b^* where domains of critical cluster size n^* are separated by black lines for (a) the square lattice and (b) the triangular lattice. The colors depict the most favorable bond counts b^*, where in larger sized domains also values for n^* are given. Note that for the square lattice all domains of constant n^* that do not extend down to $T = 0$ are split in a b^* lower and a $b^* - 1$ upper temperature region; for the triangular lattice, most domains of constant n^*, certainly those that do not extend down to $T = 0$, are split in two or three temperature regions. This indicates that for those n^* less compact shapes become more favorable in the higher temperature region compared to the lower temperature region. The boundaries of the shaded domains are not definite due to limited $n_{\max}$.

that all observed cluster sizes after a certain amount of MCSS (when starting at MCSS = 0 from the same initial input cluster) are plotted in ascending (or descending) order. In this way, for each input cluster of size n, the decay fraction $f_d^n(H,T)$ and growth fraction $f_g^n(H,T) = 1 - f_d^n$ were determined for a given temperature T and external field H. The critical cluster size n^* was then defined as the size of the input cluster that shows a decay fraction closest to 0.5:

$$n^*(H,T) = \min\left[\left|f_d^n(H,T) - f_g^n(H,T)\right|; n_{\min} \leqslant n \leqslant n_{\max}\right]. \tag{15}$$

Compared to the thermodynamic definitions provided in the previous Sec. II B the present definition of the critical cluster size based on MC simulations can thus be considered a kinetic definition.

III. RESULTS

A. Results of lattice animal enumeration

The results of the enumerations using the algorithm described in Sec. II B above are shown in Fig. 1 and are listed in Supplemental Material in Ref. 24 for both the square and triangular lattices. Cumulative data $\sum_b w_n^b$, available for both square[25] and triangular[26] lattices, were used for verification of the calculated data. Moreover, the present data for the square lattice are identical to the data presented by Ref. 8 going up to $n = 17$ (apart from a mistake in this list at $n = 12$ and $k - n + 1 = 0$; it gives 268 852, but must be 268 352), and Ref. 9 going up to $n = 21$.

Using the results given in Table I in Ref. 24, a "phase diagram" of relative temperature T/T_c versus external magnetic field H, showing domains of constant critical cluster size n^* was constructed for the square lattice; see Fig. 2(a).

Effectively, this phase diagram was already given in Ref. 8, but we extended it from $n = 17$ up to $n = 29$. In addition, we are now showing in one figure both the domains of constant critical bond count b^* using the color coding (see scale at the right-hand axis) and the domains of critical cluster size n^* as indicated by the numbers in the figure. For the triangular lattice, the analogous phase diagrams were calculated up to $n = 25$, using the results in Table II in Ref. 24, and are presented with domains of constant n^* and b^* in Fig. 2(b). Boundaries of domains that are not definite due to limited $n_{\max}$ are shaded.

For $T = 0$, the critical sizes n^* as a function of H in Fig. 2(b) are identical to the sizes calculated using the primary maxima of the energy function, e.g., as described by Eqs. (5) and (6) in Sec. II A for the triangular lattice. For the square lattice, the primary maxima correspond to the $n^* = m(m + 1)$ rectangles with an extra spin on the longer side. Also just above $T = 0$, the secondary maxima in Fig. 2(b) for the triangular lattice appear in full agreement with the calculations based on the energy function for the most compact sizes, i.e., Eqs. (7) and (8) for the triangular lattice. For the square lattice, the secondary maxima correspond to $n^* = m^2 + 1$, i.e., square clusters with an extra spin on one side. For higher temperatures (say $T > 0.2\ T_c$), a more complex pattern appears, showing small domains for which the critical cluster size decreases with increasing temperature (at a certain field H). For the triangular lattice, this complex pattern develops already at lower temperatures than for the square lattice.

When comparing the domains of constant n^* with b^* interesting behavior is observed. Let's first consider the situation for the square lattice, because this is more straightforward than for the triangular lattice. For the nonprimary and nonsecondary domains of constant n^*, i.e., those n^* domains that do not extend down to $T = 0$, two b^* regions are present within each domain of constant n^*: b^* becomes $b^* - 1$ above a certain temperature in the domain. This transition only depends on the temperature since there is no coupling between the external H field and the number of bonds [cf. Eq. (2)]. This is a clear entropic effect, because certain n^* clusters, which have a higher energy (because they contain one bond less and thus have a larger perimeter) but have a larger number of configurations w_n^b, become more favorable when the temperature is increased. For the triangular lattice, some domains of constant n^* are split (instead of two) in three temperature regions, with b^*, $b^* - 1$, and $b^* - 2$ when going to higher temperature. For instance, the domains with $n^* = 4,5,9$.

The phase diagram of T/T_c versus H, showing domains of constant critical n^*, calculated using the thermodynamically averaged distribution, are shown in Figs. 3(a) and 3(b) for the square and triangular lattices, respectively. At low temperatures (say $T < 0.2\ T_c$), the figures show identical behavior as for the microscopic definition. At higher temperatures, the domain boundaries bifurcate, creating new domains with values for the critical size n^* that are in between the ones of the neighboring domains. This creates a fine pattern with a gradually increasing n^* when going (at a certain temperature) to lower H. This also means that the magic numbers that hold for n^* at low temperatures ($T < 0.2\ T_c$) become gradually replaced by the whole spectrum of all possible integer n^* at

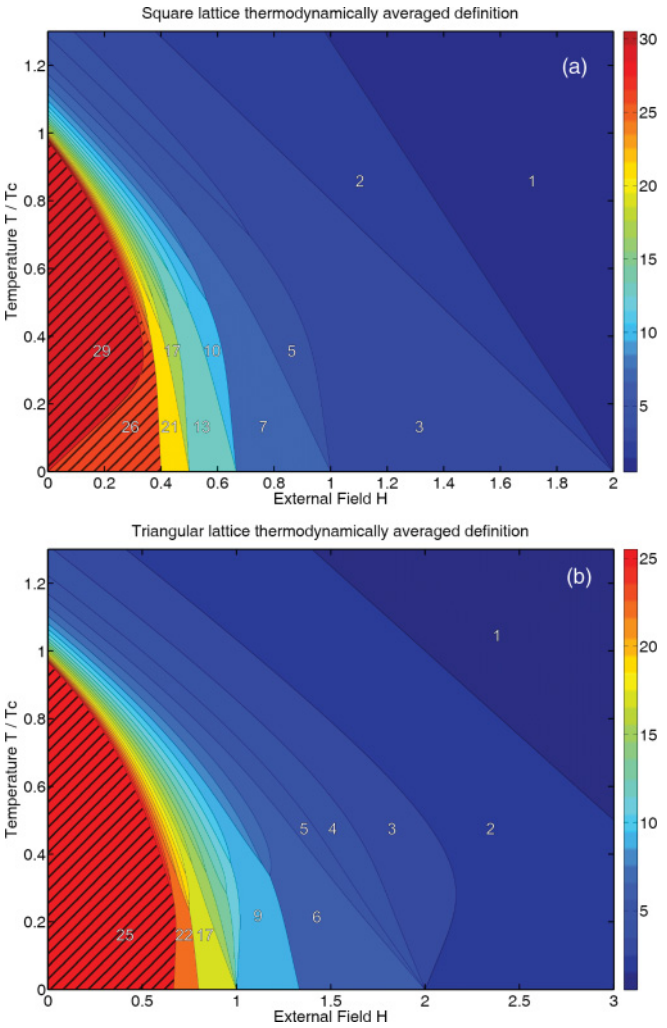

FIG. 3. (Color online) Plot of normalized temperature vs external field H showing domains of constant critical size n^* as defined by the averaged distribution [cf. Eq. (12)] for (a) the square lattice and (b) the triangular lattice. (a) Between $T = 0$ and $T = 0.3\ T_c$ the domains are similar to those in Fig. 2(a), above $0.3\ T_c$ a fine pattern appears with increasing n^* when going (at a certain temperature) to lower H. (b) Between $T = 0$ and $T = 0.2\ T_c$ the domains are similar to those in Fig. 2(b), above $0.2\ T_c$ a fine pattern appears with increasing n^* when going (at a certain temperature) to lower H. The boundaries of the shaded domains are not definite due to limited $n_{\max}$.

higher temperatures. This replacement occurs for the triangular lattice at clearly lower relative temperatures (T/T_c) than for the square lattice.

For all phase diagrams, it is clear that n^* decreases with increasing H. This is an obvious result because the maximum in (every possible) curve of E_n^b versus n [cf. Eqs. (2) and (3)] shifts to lower n for higher H. For all phase diagrams, it is also clear that n^* decreases with increasing T. The reason for this is that for lower n the total number of possible configurations is also lower. At higher temperatures, the configurational entropy term becomes increasingly determining compared to the energy term [cf. Eq. (8)]. Therefore clusters become increasingly critical when they have fewer configurations, i.e., when they are smaller. In Figs. 2 and 3, the results of the

calculations are shown for $T \geqslant Tc$, however, the assumption of $J = 1$ is not justified in this regime and the results should be treated as formal.

B. Results of Monte Carlo simulations

To determine the critical cluster sizes, using the approach employing MC simulations as delineated in Sec. II B, MC simulations were repeated with different input clusters ranging from a cluster size $n = 5$ to 32 in their most compact configuration. The simulation was run up to 40 MCSS after which the pivot point in the size distribution could clearly be determined at the intersection of the size distribution curves pertaining to 20 and 40 MCSS. The decay fraction f_d^n was taken equal to the relative position of the pivot point.

Since the MC simulations and the critical cluster size determination are computer resource intensive, they were limited to regions that showed interesting features in the figures based on the thermodynamic calculations (cf. Figs. 2 and 3), e.g., where domain boundaries bifurcate when going from lower to higher temperatures. For the triangular lattice, the external field H was in between $0.65J$ and $0.85J$, for the square lattice, H was chosen between $0.33J$ and $0.49J$. For both lattices, the temperature T ranges between 0.23 T_c and 0.5 T_c. The MC simulations were repeated 5000 times for each input cluster to obtain enough statistical data to accurately determine the growth and decay fractions.

The resulting $n^*(H,T)$ figures are plotted in Fig. 4(a) for the square lattice and in Fig. 5(a) for the triangular lattice. For both lattices, a gradual decrease in critical cluster size is found with increasing temperature and external field; both effects were already explained in Sec. III A directly above. The negative slope of the boundaries and bands of the critical sizes becomes slightly more negative when going to lower H fields.

In the phase diagram of the triangular lattice, all domains with value n^* border domains with value $n^* + 1$ or $n^* - 1$. All changes in critical size are gradual in this window. The domains get slightly narrower when going to lower H. Clearly, no sign of magic numbers can be observed.

On the square lattice, the transitions between domains are less gradual because they involve larger variations in domain width (along the H axis). Also domain bands are shared by multiple critical n^*, for example, $n^* = 19$ and 20 (or 14/15 or 24/25) are both detected critical in the same region. Apart from this, some weak signs of magic numbers are present, because the domains with $n^* = 17,21$, or 26 are wider.

These results on the critical nuclei turn out to be not sensitive to the type of inserted cluster, because results for inserted clusters on the square lattice with two internal bonds less, i.e., two corner sides of the most compact clusters were removed and added to the longer sides of the remaining cluster, showed very similar results. With respect to Fig. 4(a) only a shift in H of -0.03J is found for the critical cluster size in case of the inserted less compact clusters. No significant other changes are present in the results for the two types of input clusters and therefore the main conclusions of the present work are not dependent on the type of inserted cluster as long as they are near the appropriate growth (and decay) paths for this temperature and fields.

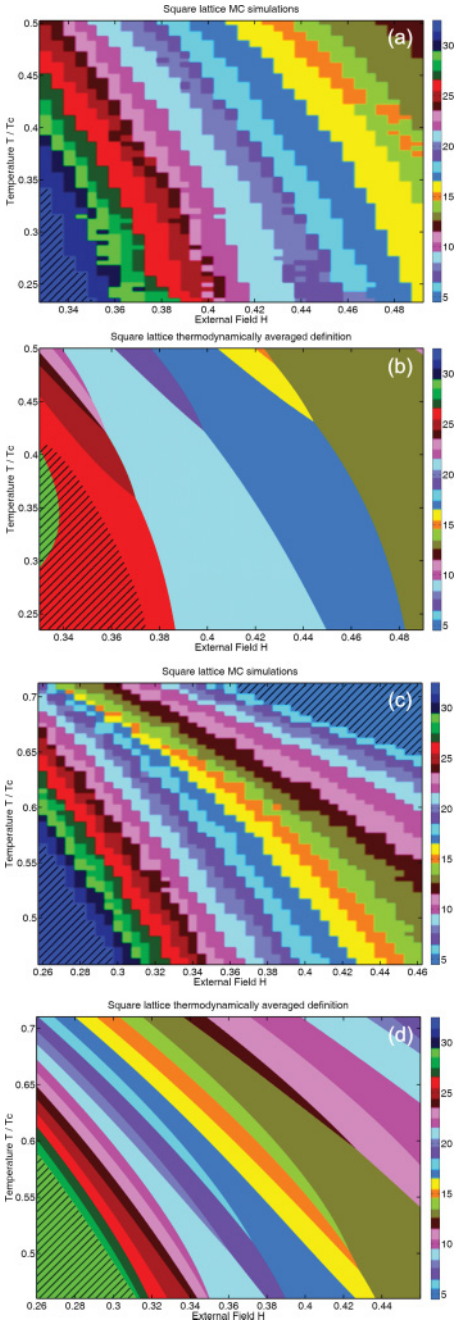

FIG. 4. (Color online) Domains for critical size n^* on a square lattice. The color indicates the critical size n^*. (a) and (b) Temperature T between 0.23 T_c and 0.50 T_c and external field H between $0.33J$ and $0.49J$. (c) and (d) Temperature T between 0.46 $T_c$and 0.71 T_c and external field H between $0.26J$ and $0.46J$. (a) and (c) For each point, 5000 clusters in their most compact configurations were used for the MC simulations for each n. For each simulation, the decay fraction was determined after 40 MCSS and was used to determine the critical cluster size n^* [cf. Eq. (15)]. (b) and (d) Critical cluster size as determined by the thermodynamically averaged definition [cf. Eq. (12b)]. The boundaries of the shaded domains are not definite due to limited $n_{\max}$.

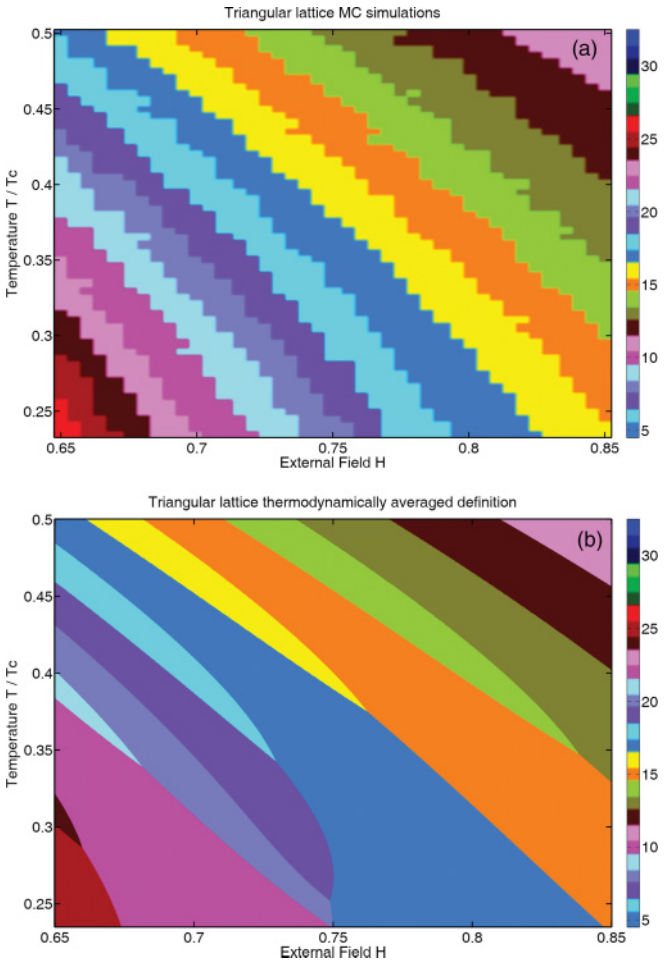

FIG. 5. (Color online) Domains for critical size n^* on a triangular lattice for T between 0.23 T_c and 0.5 T_c and H between $0.65J$ and $0.85J$. The color indicates the critical size n^*. (a) Results from the Monte Carlo simulations. For each point, 5000 clusters in their most compact configurations were used for the MC simulations for each n. For each simulation, the decay fraction was determined after 40 MCSS and was used to determine the critical cluster size n^* [cf. Eq. (15)]. (b) Results from the averaged definition as calculated using Eq. (12a).

C. Comparing results of lattice animal enumeration and Monte Carlo simulations

When comparing the domain maps based on the thermodynamic definitions with the ones derived using the MC simulations, it is seen that the best agreement is found with the thermodynamically averaged distribution, see Figs. 4 and 5. No large discrete regions are observed in the MC simulations, similar as seen for the saddle-point definition. Instead, there are bands of constant critical size with an increasing negative slope for higher H, like in the case of the thermodynamically averaged results. This holds for both the triangular and square lattices. This is an interesting observation because the starting clusters for the MC simulations are the most compact shapes (closest to perfect square or hexagonal shapes) and therefore these clusters start directly on the lowest energy path associated with the saddle-point definition. Apparently, during the MC simulations, an averaging over configurations is taking place that appears to go away from the lowest energy path and, as we will show below, the averaging is even going beyond the one of the thermodynamically averaged result.

For the square lattice, not all critical sizes are present in the MC simulations in similar quantities. For example, input clusters of size 20 and 25 are less present than clusters of size 21 and 26. This is supported by the thermodynamically determined critical sizes where below 0.36 T_c no critical size of 25 is found. A big difference is, however, that even at a low temperature of $0.25T_c$ all possible critical sizes (in the interval 12–32) are still found in the MC simulations, whereas in the thermodynamic definition only the magic numbers 13, 17, 21, and 26 are present.

By increasing the temperature T to the range of 0.46 T_c to 0.71 T_c and decreasing the external field H to the range of 0.26 to 0.46 the thermodynamically averaged definition shows a gradual change from large clusters to small ones with all possible n^* present, see Figs. 4(c) and 4(d). MC simulations on a square lattice performed in this range show excellent agreement for clusters larger than $n^* = 15$ for the entire range, while for smaller cluster sizes the best agreement is found for $T < 0.6\ T_c$ (and $T > 0.45\ T_c$).

For the triangular lattice, we see an excellent agreement between the MC simulations and the results from the averaged definition for temperatures above 0.4 T_c, see Fig. 5. Below this temperature, the domains according to the thermodynamically averaged definition gradually reduce to only the ones of the magic numbers described by Eqs. (6)–(9), whereas the MC simulations still shows the presence of all possible n^*.

Apparently, for both the square and triangular lattices at low temperatures ($<\sim 0.30\ T_c$ for the range of H values presented), the MC simulations still provide the complete spectrum of all possible n^* and are not following the results for the thermodynamically averaged definition of the critical cluster size. The reason for this is that with the MC definition of the critical cluster size, i.e., the most compact n-size cluster that has a probability to grow (or decay) most closely to 50%, not only averaging over b for a certain n takes place, but that also a certain weighted averaging over directly associated neighboring n takes place. In this respect, it is quite obvious that the occurrence of magic numbers for the critical cluster size is strongly suppressed according to the kinetic MC definition. In this respect, the MC simulations provide results that show some interesting features also predicted by the transition path theory.[15]

D. Temperature evolution of magic numbers according to Monte Carlo simulations

The MC simulations indicate that magic numbers are not present at low temperatures such as $T/T_c = 0.25$, at least not in the sequence of critical nuclei as a function of magnetic field H. Moreover, the phase diagrams shown above in Figs. 2 and 3 indicate that the disappearance of magic numbers with temperature increase occurs at lower temperatures for the triangular lattice than for the square one. To shed more light on these issues, Fig. 6 presents cluster-size distributions obtained by MC simulations at relatively low temperatures for the square and triangular lattices, where on both lattices the starting cluster was a $n = 30$ cluster in (one of) its

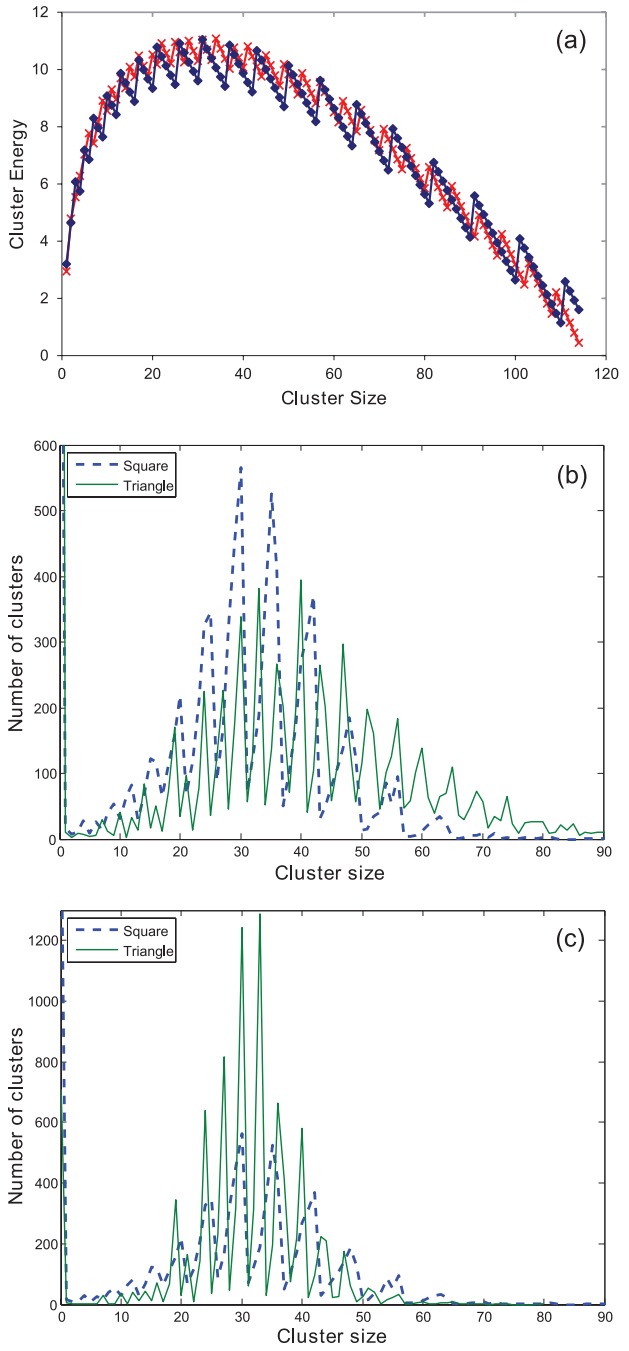

FIG. 6. (Color online) (a) Cluster energy E_n^b normalized by T_c as a function of cluster size n for both square (diamonds) and triangular (crosses) lattice for the most compact clusters. The external field H was chosen such that the energy curves for the triangular and square lattices obtain the same overall shape. (b) Cluster size distribution at $T = 0.454$ K after 200 MCSS (square lattice) and 300 MCSS (triangular lattice) after insertion of a most compact $n = 30$ cluster. For both lattices, the occurrence of magic numbers is clearly visible, but the modulation is clearly stronger for the square lattice. (c) Cluster size distribution for the triangular lattice at $T = 0.377$ K after 400 MCSS. For the square lattice the distribution is identical as in (b), i.e., holds for $T = 0.454$ K after 200 MCSS. This difference in temperature for both lattices ensures that the height in the saw tooth modulation of the energy curve shown in (a) is the same for both cases. Now the magic numbers are more prominent for the triangular than for the square lattice.

most compact shape. The statistic distribution of cluster sizes obtained for 10000 initially identical clusters is shown after a sufficiently large number of MCSS, which allows some local equilibration of cluster sizes. Actually, the cluster size distribution can be considered the product of a Gaussian distribution with the semiequilibrium distribution described by Eq. (10).[14] For fixed H and T, Eq. (10) is fixed, but the Gaussian distribution evolves with MCSS from nearly a δ function to a broad distribution.

Figure 6(a) shows, for both the triangular and square lattices, the cluster energy E_n^b normalized by the critical temperature T_c as a function of cluster size n for the most compact clusters (i.e., largest number of bonds b) and thus depicts the lowest energy path for growing (and decaying) clusters. The energy curves in Fig. 6(a) clearly exhibit an overall classical (Gibbs) outlook plus a sharp saw-tooth modulation. The values for H were chosen such that the overall classical outlook of the energy curves for the triangular and square lattice obtains the same shape, with a maximum near $n = 30$, i.e., $H = 0.37$ for the square lattice and $H = 0.642$ for the triangular lattice. Normalization by T_c allows the energy curves to also obtain comparable absolute values. In this way, we create comparable energy landscapes for cluster evolution on the triangular and square lattice.

Figure 6(b) shows results for $T = 0.454$, i.e., the same absolute temperature for the square and triangular lattices (which is $T = 0.2\ T_c$ for the square and $T = 0.1247\ T_c$ for the triangular lattice). The results for the square lattice hold after 200 MCSS and for the triangular lattice after 300 MCSS, but the conclusions we will draw below are not sensitive to the value of the MCSS. In both cluster size distributions, clear signs of the expected magic numbers for maxima and minima are present. These magic numbers vanish at approximately $0.2\ T_c$ for the triangular lattice and $0.4\ T_c$ for the square lattice. Despite that T/T_c is clearly lower for the triangular lattice, the (amplitude of the) modulation in the size distribution, i.e., the ratio between neighboring maxima and minima, is clearly smaller in case of the triangular lattice than for the square lattice. The main reason for this is that, for the same absolute temperature, the value for the saw-tooth modulation (barrier heights) in the energy curve E_n^b versus n is lower for the triangular than for the one of square lattice case [cf. Fig. 6(a)].

Therefore it is interesting to lower the temperature for the triangular lattice such that the same value for the saw-tooth modulation holds for the (lowest-energy path in the) E_n^b versus n curves of the square and triangular lattices. To do so, the temperature is reduced from $T = 0.1247\ T_c$ [the case shown in Fig. 6(b)] to $T = 0.1038\ T_c$ and the result (after 400 MCSS) is shown in Fig. 6(c). The size distribution holding for the square lattice is the same in Figs. 6(b) and 6(c). Lowering the temperature of the triangular lattice has the clear effect that the modulation and magic numbers (which were weaker) are now much stronger present in the size distribution for the triangular lattice than for the square one. Apparently, for the same value of the saw-tooth modulation (barrier heights) in the energy path, the lower absolute temperature for the triangular lattice determines that the modulation in the size distribution and thus the magic numbers become more prominent. This can be understood because the lower the temperatures, the more growth proceeds via the lowest-energy

path. At higher temperatures, growth also occurs via less favorable (higher energy) cluster configurations, which obscure the magic numbers (and thus dampens the modulation) in the size distribution.

Despite that magic numbers are *not* present according to the kinetic MC definition of critical cluster sizes (see previous section), the present results show that they are actually present in the size distribution itself for the square lattice below about 0.4 T_c (for $\sim 0.3J < H <\sim 0.5J$) and for the triangular lattice below $\sim$0.2 T_c (for $\sim 0.5J < H <\sim 0.9J$).

The question now remains when magic numbers will become present according to the kinetic MC definition of critical cluster sizes. To test this, additional MC simulations were performed for the square lattice for $T = 0.15\ T_c$ for H between $0.1J$ and 0.5J with 1000 MCSS and showed that the critical clusters as found from theory $[m^*(m^*+1)+1$ and $m^2+1]$ are clearly present. Cluster sizes in between these critical cluster sizes were also present but only in thin lines between the critical domains. Therefore we expect that the critical cluster sizes according to our kinetic definition will also converge to, i.e., reproduce the sizes with magic numbers of the exact results of Neves Schonmann for $T \to 0$.

The present results show some interesting agreement with predictions of the transition path theory (TPT).[15] TPT shows, for example, that at elevated temperatures a critical cluster size for nucleation is not present, but there is a transition path region (which includes many different clusters also with different sizes). Therefore, from TPT, at higher T a "critical cluster size for nucleation" in the Ising model can be absent, but when $T \to 0$ the transition path region converge exactly to the critical nuclei according to Neves Schonmann.[16] These predictions agree very well with the results of our MC simulations described and shown above. It is particularly relevant to note that at higher temperatures the averaging over neighboring cluster sizes indicates that, in principle, there is no critical cluster size, but only a transition path region. The results also show that the thermodynamic definitions have limited meaning. The saddle-point definition is only relevant for $T \to 0$.

E. Reduced interface tension according to lattice animals

An interesting correlation can be made between the disappearance of magic numbers with temperature increase in the size distributions and the disappearance of the difference in interface tension for the lowest and highest interface energy direction of the Ising system considered. For the square lattice, the lowest interface tension holds for the direction parallel to one of the two principal lattice vectors (i.e., parallel to a {10} boundary):[27]

$$\sigma_{//} = 2 + T \ln\left[\tanh\left(\frac{1}{T}\right)\right]. \tag{16a}$$

The highest interface tension holds for the two directions making 45° with the principal lattice vectors (i.e., parallel to a {11} boundary):[27]

$$\sigma_{\text{diag}} = T\sqrt{2}\sinh\left(\frac{2}{T}\right). \tag{16b}$$

These two interface tensions are shown as a function of reduced temperature [i.e., with $T_c = 2/\ln(\sqrt{2}+1)$] in Fig. 7(a). For temperatures above 0.6 T_c, about the same interface energies hold for $\sigma_{//}$ and σ_{diag}. In the range from 0.6 T_c down to 0.3 T_c, the difference between the highest and lowest interface energy is still modest, but this difference rapidly increases when going from 0.3 T_c down to 0 T_c.

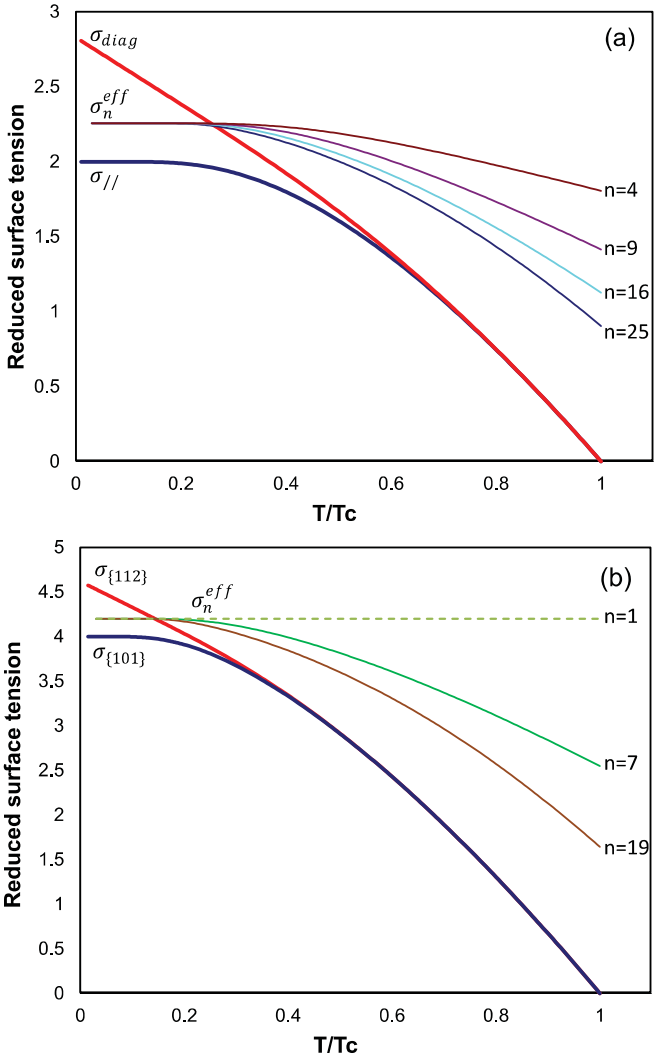

FIG. 7. (Color online) Lowest and highest interface tension as a function of normalized temperature compared with the effective interface tension derived from the results of the lattice-animals enumeration for the most compact square and hexagonal clusters. (a) For the square lattice, the lowest interface and the highest interface tension hold for the directions parallel and making a 45° angle with the principal lattice vectors: $\sigma_{//}$ and σ_{diag}. Above 0.6 T_c about the same interface energy is found for $\sigma_{//}$ and σ_{diag}, below 0.6 T_c a modest difference is seen, which is rapidly increasing below 0.3 T_c. (b) For the triangular lattice, the lowest interface tension and the highest interface tension hold for the parallel direction that makes a 30° angle with the principal lattice vectors: $\sigma_{\{10\bar{1}\}}$ and $\sigma_{\{11\bar{2}\}}$. Above 0.3 T_c, about the same interface energy is found for $\sigma_{\{10\bar{1}\}}$ and $\sigma_{\{11\bar{2}\}}$, below 0.3 T_c, a modest difference is seen, which is rapidly increasing below 0.15 T_c.

For the triangular lattice, the lowest interfacial tension holds for the direction parallel to one of the three principal lattice

vectors (i.e., parallel to the $\{10\bar{1}\}$ boundary):[28]

$$\sigma_{\{10\bar{1}\}} = 2T\,\mathrm{arccosh}\left(\sqrt{\frac{2X+3}{4}} - \frac{1}{2}\right). \tag{17a}$$

The highest interfacial tension holds for the three directions making 30° with the principle lattice vectors (i.e. parallel to the $\{11\bar{2}\}$ boundary):[28]

$$\sigma_{\{11\bar{2}\}} = \frac{2T}{\sqrt{3}}\mathrm{arccosh}\left(\frac{X-1}{2}\right), \tag{17b}$$

with X specified as

$$X = \frac{2y}{(1-y)^2} + \frac{(1-y)^2}{2y} + 1, \tag{17c}$$

and with y specified as

$$y = \tanh\left(J/T\right). \tag{17d}$$

These two interface tensions are shown as a function of reduced temperature [i.e., with $T_c = 4/\ln(3)$] in Fig. 7(b). For temperatures above $0.3\ T_c$, about the same interface energies hold for $\sigma_{\{10\bar{1}\}}$ and $\sigma_{\{11\bar{2}\}}$. In the range from $0.3\ T_c$ down to $0.15\ T_c$, the difference between the highest and lowest interface energy is still modest, but this difference rapidly increases when going from $0.15\ T_c$ down to $0\ T_c$.

Interestingly, the difference in highest and lowest interface tension lattice reduces to a value of about 0.12 at $0.4\ T_c$ for the square lattice and at $0.2\ T_c$ for the triangular lattice. Apparently, at these temperatures the experienced anisotropy in interface tension is so low that also in the MC simulations the magic numbers disappear. The evolution and the disappearance of the difference in interface tension occur at two times higher T/T_c values for the square than for the triangular lattice. The same holds for the evolution and disappearance of magic cluster sizes with the MC simulations. Therefore an interesting correlation exists between the disappearance of anisotropy in interface tension with temperature increase holding for the Ising systems considered and the disappearance of magic numbers with temperature rise based on MC simulations of these Ising systems.

Partly, the comparison between the interfacial tension and the MC simulations is not appropriate, because with the MC simulations we consider (too) small cluster sizes. This can be readily deduced from the following analysis. Using the results of the lattice animal enumeration, we are able to derive an effective interface tension associated with a certain cluster size, which is defined for the square lattice as[27]

$$\sigma_n^{s,\mathrm{eff}} = \frac{-T\ln\left(\sum_{b_{\min}}^{b_{\max}} D_n^b\right)}{2\sqrt{\pi n}} \tag{18}$$

and for the triangular lattice as

$$\sigma_n^{t,\mathrm{eff}} = \frac{-T\ln\left(\sum_{b_{\min}}^{b_{\max}} D_n^b\right)}{\sqrt{\sqrt{3}\pi(4n-1)/2}}, \tag{19}$$

where D_n^b is given by Eq. (10) for $H = 0$. This effectively means that the cluster area (independent of shape) is mapped onto a circle and the circumference of this circle is taken as the interface length. The size-dependent effective interface tensions are shown for most compact shapes in Figs. 7(a) and 7(b) for the square and triangular lattices, respectively. Clearly, it can be observed that the effective interface tensions of these small clusters largely deviate from the ones of long interfaces according to the Ising models considered. Since hexagons have shapes better approaching the circular circumference than squares, it might be expected that in the high-temperature regime, where there is no anisotropy in interface tension for long interfaces, the effective interface tension with increasing cluster size more rapidly converges to the one of long interfaces. The present results do not show this more rapid convergence as a function of cluster size n, but when normalized to the facet length of the hexagon and square (so that hexagons with $n = 7$ and 19 are compared to squares with $n = 4$ and 9, respectively) indeed this more rapid convergence occurs.

IV. SUMMARY AND CONCLUSIONS

In the present work, we have studied the growth and decay of clusters at temperatures below T_c for a two-dimensional Ising model on square and triangular lattices. This was done by enumerating all unique lattice configurations up to $n = 25$ for the triangular lattice and up to $n = 29$ for the square lattice. From these enumerations, the critical cluster sizes as a function of temperature and external field have been calculated for both lattices using two different thermodynamic definitions. In addition, Monte Carlo simulations were performed to calculate the critical cluster size using a kinetic definition. By inserting a (most) compact cluster at the start of the simulation on a relatively small lattice, the simulation was speeded up at low temperatures.

The obtained MC results are in good agreement with the results obtained from the lattice animal enumeration based on the thermodynamic "averaged" definition. In contrast, the thermodynamic saddle-point definition provides results that strongly deviate from the other two definitions at higher temperatures ($T >\sim 0.4\ T_c$ for $\sim 0.3J < H <\sim 0.5J$ for the square lattice and $T >\sim 0.2\ T_c$ for $\sim 0.5J < H <\sim 0.9J$ for the triangular lattice). Even when we start with the inserted most compact cluster exactly in the saddle point of the energy landscape, still the MC simulations will create a critical cluster size based on averaging not only over the various highest bond numbers for this size, but also influenced by growth and decay of neighboring cluster sizes. These results show interesting correspondence with predictions of TPT. The dominance of a transition path region is also the principle reason that magic numbers found at low temperatures in the critical cluster size mapping determined from the lattice animal enumeration did not appear in the results from the MC simulations. However, the magic numbers are still present at these low temperatures when looking at the cluster size distributions themselves during the MC simulation. Magic numbers in the size distribution are absent for $T >\sim 0.4\ T_c$ for the square lattice and $T >\sim 0.2\ T_c$ for the triangular lattice. This disappearance of the magic numbers with temperature increase according to the MC simulations appears to correlate well with the disappearance of anisotropy in interface tension for both the triangular and square lattice Ising models.

ACKNOWLEDGMENTS

This research was carried out under project number M62.7.08SDMP03 in the framework of the Industrial Partnership Program on Size Dependent Material Properties of the Materials innovation institute M2i and the Foundation of Fundamental Research on Matter (FOM), which is part of the Netherlands Organisation for Scientific Research.

*gerteising@gmail.com

†b.j.kooi@rug.nl

[1] *Phase Transitions in the Early Universe: Theory and Observations*, edited by Héctor J. Vega, Isaak Markovich Khalatnikov, and Norma Sánchez, NATO Science Series, II Mathematics, Physics, and Chemistry Vol. 40 (Kluwer Academic Publishers, Dordrecht, The Netherlands, 2001); A. B. C. Patzer, A. Gauger, and E. Sedlmayr, Astron. Astrophys. **337**, 847 (1998); Takaya Nozawa, Takashi Kozasa, Hideyuki Umeda, Keiichi Maeda, and Ken'ichi Nomoto, Astrophys. J. **598**, 785 (2003); I. Bombaci, D. Logoteta, C. Providência, and I. Vidaña, Astron. Astrophys. **528**, A71 (2011).

[2] R. McGraw and Y. Liu, Phys. Rev. Lett. **90**, 018501 (2003).

[3] J. W. Christian, *The Theory of Transformations in Metals and Alloys* (Pergamon, Oxford, UK, 2002); David A. Porter, K. E. Easterling, and Mohamed Y. Sherif, *Phase Transformations in Metals and Alloys* (CRC Press, Boca Raton, FL, 2009).

[4] *Nucleation Theory and Applications*, edited by J. Schmelzer (Wiley, New York, 2005).

[5] Bong-Sub Lee, G. W. Burr, R. M. Shelby, S. Raoux, C. T. Rettner, S. N. Bogle, K. Darmawikarta, S. G. Bishop, and J. R. Abelson, Science **326**, 980 (2009).

[6] K. F. Kelton, A. L. Greer, and C. V. Thompson, J. Chem. Phys. **79**, 6261 (1983).

[7] V. A. Shneidman, J. Stat. Phys. **112**, 293 (2003).

[8] V. A. Shneidmann and G. M. Nita, J. Chem. Phys. **121**, 11232 (2004).

[9] S. Frank, D. E. Roberts, and P. A. Rikvold, J. Chem. Phys. **122**, 064705 (2005).

[10] S. Ryu and W. Cai, Phys. Rev. E **81**, 030601 (2010)

[11] K. Binder and H. Müller-Krumbhaar, Phys. Rev. B **9**, 2328 (1974).

[12] P. A. Rikvold, H. Tomita, S. Miyashita, and S. W. Sides, Phys. Rev. E **49**, 5080 (1994); V. A. Shneidman, K. A. Jackson, and K. M. Beatty, Phys. Rev. B **59**, 3579 (1999).

[13] A. Bovier and F. Manzo, J. Stat. Phys. **107**, 757 (2002); K. Park, P. A. Rikvold, G. M. Buendia, and M. A. Novotny, Phys. Rev. Lett. **92**, 015701 (2004); G. M. Buendia, P. A. Rikvold, K. Park, and M. A. Novotny, J. Chem. Phys. **121**, 4193 (2004); V. A. Shneidman and G. M. Nita, Phys. Rev. Lett. **89**, 025701 (2002); K. Brendel, G. T. Barkema, and H. van Beijeren, Phys. Rev. E **71**, 031601 (2005); R. J. Allen, C. Valeriani, S. Tanase-Nicola, P. R. ten Wolde, and D. Frenkel, J. Chem. Phys. **129**, 134704 (2008); W. R. Deskins, G. Brown, S. H. Thompson, and P. A. Rikvold, Phys. Rev. B **84**, 094431 (2011).

[14] B. J. Kooi, Phys. Rev. B **77**, 024303 (2008).

[15] P. G. Bolhuis, D. Chandler, C. Dellago, and P. L. Geissler, Annu. Rev. Phys. Chem. **53**, 291 (2002); W. E, W. Ren, and E. Vanden-Eijnden, J. Phys. Chem. B **109**, 6688 (2005); Phys. Rev. B **66**, 052301 (2002); E. Vanden-Eijnden, in *Computer Simulations in Condensed Matter Systems: From Materials to Chemical Biology Volume 1*, edited by M. Ferrario, G. Ciccotti, and K. Binder, Lecture Notes in Physics Vol. 703 (Springer, Berlin, Heidelberg, 2006), pp. 453–493.

[16] E. J. Neves and R. H. Schonmann, Commun. Math. Phys. **137**(2), 209 (1991).

[17] S. Redner, J. Stat. Phys. **29**, 309 (1982).

[18] S. Mertens, J. Stat. Phys. **66**, 669 (1992).

[19] L. Onsager, Phys. Rev. **65**, 117 (1944).

[20] R. M. F. Houtappel, Physica A **16**, 425 (1950).

[21] R. J. Glauber, J. Math. Phys. **4**, 294 (1963).

[22] R. A. Ramos, P. A. Rikvold, and M. A. Novotny, Phys. Rev. B **59**, 9053 (1999); B. J. Kooi, *ibid.* **73**, 054103 (2006).

[23] J. Hoshen and R. Kopelman, Phys. Rev. B **14**, 3438 (1976).

[24] See Supplemental Material at http://link.aps.org/supplemental/10.1103/PhysRevB.85.214108 for a listing of the number of unique lattice animals by size and bond count for the square lattice (up to $n = 29$) and the triangular lattice (up to $n = 25$).

[25] I. Jensen, J. Stat. Phys. **102**, 865 (2001).

[26] M. Vöge and A. J. Guttmann, Theor. Comp. Sci. **307**, 433 (2003).

[27] V. A. Shneidman, K. A. Jackson, and K. M. Beatty, J. Chem. Phys. **111**, 6932 (1999).

[28] V. A. Shneidman and R. K. P. Zia, Phys. Rev. B **63**, 085410 (2001).